

Article

Extensive Analysis of a Reinvigorated Solar Water Heating System Using Low-Density Polyethylene Glazing

Balamurali Duraivel¹, Natarajan Muthuswamy¹, Saboor Shaik¹ , Erdem Cuce^{2,3,4} ,
Abdulhameed Babatunde Owolabi^{5,6,*} , Hong Xian Li⁷ and Miroslava Kavgić⁸

- ¹ Department of Thermal and Energy Engineering, School of Mechanical Engineering, Vellore Institute of Technology, Vellore 632 014, India; balzzz07@gmail.com (B.D.); m.natarajan@vit.ac.in (N.M.); saboor.nitk@gmail.com (S.S.)
 - ² Low/Zero Carbon Energy Technologies Laboratory, Faculty of Engineering and Architecture, Recep Tayyip Erdogan University, Zihni Derin Campus, 53100 Rize, Turkey; erdem.cuce@erdogan.edu.tr
 - ³ Department of Mechanical Engineering, Faculty of Engineering and Architecture, Recep Tayyip Erdogan University, Zihni Derin Campus, 53100 Rize, Turkey
 - ⁴ School of Engineering and the Built Environment, Birmingham City University, Birmingham B4 7XG, UK
 - ⁵ Regional Leading Research Center for Smart Energy System, Kyungpook National University, Sangju 37224, Republic of Korea
 - ⁶ Department of Convergence and Fusion System Engineering, Kyungpook National University, Sangju 37224, Republic of Korea
 - ⁷ School of Architecture and Built Environment, Deakin University, Geelong Waterfront Campus, Geelong 3220, Australia; hong.li@deakin.edu.au
 - ⁸ Civil Engineering Department, University of Ottawa, 161 Louis Pasteur, Ottawa, ON K1N 6N5, Canada; mkavgi@uottawa.ca
- * Correspondence: owolabiabdulhameed@gmail.com

Abstract: Solar energy is one of the most promising forms of alternative energy because it has no adverse effects on the environment and is entirely free. Converting solar energy into thermal energy is the most common and straightforward method; the efficiency of solar thermal conversion is approximately 70 percent. The intermittent nature of solar energy availability affects the performance of solar water heaters (SWH), which lowers the usefulness of solar energy in residential and commercial settings, particularly for water heating. Even at low temperatures, the performance of a collector can be improved by using low-density polyethylene (LDPE) glazing instead of traditional glass because it is less expensive and lighter than glass. Using a comprehensive experimental-simulative study, the Glass Solar water heater (glass SWH) and the low-density polyethylene solar water heater (LDPE SWH) are analyzed, examined, and compared in this work. These solar water heaters have galvanized iron (GI) as their absorber material. The SWHs were operated in a closed loop at a constant mass flow rate of 0.013 kg/s, and a 4E analysis (which stands for energy, exergy, economics, and efficiency recovery ratio) was carried out. This analysis included a look at the dynamic time, uncertainty, weight reduction, carbon footprint, and series connection. An LDPE SWH has an energy efficiency that is 5.57% and an exergy efficiency that is 3.2% higher than a glass SWH. The weight of the LDPE SWH is 32.56% lower than that of the glass SWH. Compared to the price of a conventional geyser, installing our SWH results in a cost savings of 40.9%, and monthly energy costs are reduced by an average of 25.5%. Compared to October, September has the quickest dynamic time to reach the desired temperature, while October has the most significant dynamic time. The efficiency recovery ratio (ERR) of a glass SWH is 0.0239% lower than that of an LDPE SWH. LDPE SWHs had a carbon credit worth INR 294.44 more than glass SWHs. The findings of these tests demonstrate that the LDPE SWH is a practical replacement for traditional means of heating water, such as SWHs and geysers.

Keywords: flat plate solar water heater; transmissivity; low-density polyethylene (LDPE) glazing; exergy efficiency; recovery efficiency ratio; dynamic time; carbon footprint



Citation: Duraivel, B.; Muthuswamy, N.; Shaik, S.; Cuce, E.; Owolabi, A.B.; Li, H.X.; Kavgić, M. Extensive Analysis of a Reinvigorated Solar Water Heating System Using Low-Density Polyethylene Glazing. *Energies* **2023**, *16*, 5902. <https://doi.org/10.3390/en16165902>

Academic Editor: F. Pacheco Torgal

Received: 11 July 2023

Revised: 2 August 2023

Accepted: 5 August 2023

Published: 9 August 2023



Copyright: © 2023 by the authors. Licensee MDPI, Basel, Switzerland. This article is an open access article distributed under the terms and conditions of the Creative Commons Attribution (CC BY) license (<https://creativecommons.org/licenses/by/4.0/>).

1. Introduction

These days, solar power ranks high on the list of the world's most important renewable energies [1]. India's strategic positioning between the equator and the tropic of Cancer ($68^{\circ}7'$ to $97^{\circ}25'$ east longitude and 84° to $37^{\circ}6'$ north latitude) gives a wealth of solar resources. Because of this, it is necessary to create tools that make the most of solar power. Solar energy can be transformed into thermal energy using a certain kind of heat exchanger as a thermal solar collector. Flat plate collectors are the most prevalent of the many distinct types of solar collectors invented [2]. The daily availability of solar radiation makes flat plate collectors essential home equipment for heating water [3]. A flat plate collector comprises three main components: an absorber plate, a transparent cover (glazing) that lets short wave radiation pass through but blocks it from leaving, and insulation that prevents heat from escaping from the collector's back and sides. Together, the components of a flat plate collector perform three functions: they collect solar radiation, convert it to heat energy, and transfer the energy to a working fluid flowing through the collector duct [4]. Flat plate collectors use the "thermosiphon" principle [5]. The thermosiphon principle utilizes the motive forces of natural convection and conduction. These forces are used to create a cyclic fluid flow from areas of high heat to low heat and back.

Based on the thermosiphon principle, the collector absorbs solar energy and transfers thermal energy from the sun into the working fluid. The warming of the working fluid reduces its density, causing it to climb through the system. The cooled substrate falls down the opposite side of the loop and into the collector [6]. In 2020, India's solar thermal sector added 10% less capacity due to COVID-19. In 2020, India added about 1.634 million m^2 of collector area, which is less than in 2019, and this negative trend persists. Therefore, it is vital to help the market recover by appealing to local consumers. Our work focuses on enhancing the flat plate collector's affordability and efficiency, which are the primary and most important factors for a residential user to consider.

Balaram Kundu [7] studied how different absorber material profiles affect flat plate collector efficiency. The results showed that a rectangular profile (base thickness—0.17633 m, tip thickness—0.04656 m, and efficiency—61.85%) with a minor thickness variation is the best option. The authors investigated heat transfer rate enhancement strategies by using nanofluids (bare dispersion of Carbon Nano Tubes (CNT) and dispersion with Sodium Dodecyl Sulfate (SDS)). CNT/SDS has high thermal efficiency because the concentration drops by only 10% compared to bare CNT, which drops by 50% [8]. Investigation of the heat transfer rate of a flat plate collector at various Reynolds numbers (Re) by inserting twisted tapes (twist pitch to tube diameter: 3–12) was conducted in 2000. Compared to a plane SWH, the results show that decreasing the twist-pitch to tube diameter ratio at $Re \approx 12,000$ increases the heat transfer rate by up to 30% and reduces pressure drop [9]. J. El Andy et al. [10] studied black-painted solar collectors with electrodeposited bright nickel nanoparticles on copper substrates. The collector outperformed conventional collectors (overall heat loss of 2.7%; optical gain of only 19.3). Hellstrom et al. [11] say flat plate collector optics affect annual performance. After adding Teflon honeycomb and anti-reflective cover glass, they tested solar absorption and heat emittance. Emittance dropped from 0.10 to 0.05, and absorbance rose from 0.95 to 0.97, boosting the annual performance by 6.7%. M. Natarajan et al. [12] measured Vellore's monthly global radiation using 21 models in which Veeran and Page models were accurate. Authors have estimated India's monthly solar radiation using the Irrana-Bapat model. Out of 57 locations, the model had a statistically significant Root Mean Square Error (RMSE) of less than 10%, making it suitable for measuring in many parts of India [13]. Gangane et al. [14] developed a low-cost SWH by substituting aluminum for copper at a fabrication cost of INR 11,120 and a maximum outlet temperature of about 78° C. Can Ertekin et al. [15] studied SWHs in 129 locations across Turkey by comparing three types of collectors in terms of absorber materials (galvanized sheet, copper, and selective absorber, whose cost was 490.89, 615.19 and 740.49 USD, respectively). With significant performance, the payback period of galvanized iron was short. Very few studies

have been conducted to predict Vellore's solar radiation, and galvanized iron (GI) is used only for absorber sheets and tubes in very few cases.

Because the collector's sides and back are often highly insulated, the transparent cover (glazing) accounts for most heat losses in the collector. As a result, the glazing material is critical for the flat plate collector's thermal performance. The most popular glazing material, glass, transmits 90% of the incoming short-wave radiation; while transmitting, almost none of the long-wave radiation that the absorber plate emits escapes outward. The thickness of the glass glazing should be at least 3.3 mm [16]. Only a few researches have been published on the effect of glazing material thickness on solar collector performance. Flat plate collectors were tested with glass glazing of four different thicknesses (3 mm, 4 mm, 5 mm, and 6 mm) by Ramadhani Bhakari et al., and they concluded that the use of 4 mm glass glazing enhanced the performance by 7.6% [17]. However, utilizing 4 mm glass glazing during manufacture increases the chance of glass breakage, which adds to the expense. Plastic glazing could be used in place of glass glazing. A plastic cover has higher short- and long-wave transmittance and, thus, higher performance than a glass cover. Plastics' key advantages are their resistance to breaking, lightweight, and low cost [18].

Long-term research into using low-density polyethylene (LDPE) as glazing is underway. However, research on the solar transmissivity of LDPE and the performance of solar water heaters (SWH) with LDPE glazing is lacking. This work is unique in that it replaces conventional glass glazing of a solar water heater (SWH) with low-density polyethylene (LDPE) glazing, as well as changing the absorber plate and heat transfer tube material from copper to galvanized iron (GI) for efficiently and affordably satisfying domestic hot water needs. The current study will use testing and simulation to evaluate, analyze, and compare the performance of LDPE and glass-glazed SWHs with GI absorbers to that of standard electric geysers. To the best of the authors' knowledge, this is one of the few attempts to include a thorough investigation into the reaction of SWHs using LDPE as glazing and GI as the absorber.

2. Experimental Methods

2.1. Solar Radiation Analysis

The study workflow is shown in Figure 1. Any solar energy system should start with a review of solar radiation statistics [19]. Vellore lacks a weather station that can measure long-term sun radiation on the horizontal surface. Estimating solar radiation requires models and empirical correlations. The Gopinathan correlation, which was chosen from 13 solar radiation models and correlations, is more applicable for Vellore [20–22]. Vellore's 2018 solar radiation was calculated in MATLAB R2020a using Gopinathan correlation and climatic data from Brahmapuram, Vellore, on middays each month (defined by Klien [23]). Solar radiation was measured using pyranometers (Make: LPPYRA 02, Logic Energy, New Delhi, India, Accuracy: 1.5%) and pyrheliometers (Make: DR30-D1, Hukseflux Thermal Sensors, Haryana, India, Accuracy: 1.2%). Figure 2 shows the solar radiation of Vellore in 2018; it compared Vellore's theoretical and experimental solar radiation in 2018, and the values agree. The maximum radiation level was 24,000 KJ/m² in April, and the lowest was 19,000 KJ/m² in December. Equation (1) [24] provides the Gopinathan correlation.

$$\frac{H_g}{H_0} = \dot{a} + \dot{b} \left[\frac{\dot{S}}{S_{max}} \right] \quad (1)$$

where \underline{H}_g is the monthly average daily global radiation on the horizontal surface (KJ/m²-day), \underline{H}_0 is the monthly average extraterrestrial radiation, \dot{S} is the monthly average sunshine hours, S_{max} is the monthly average possible sunshine hours, and \dot{a} and \dot{b} are functions of latitude, elevation, and sunshine hours.

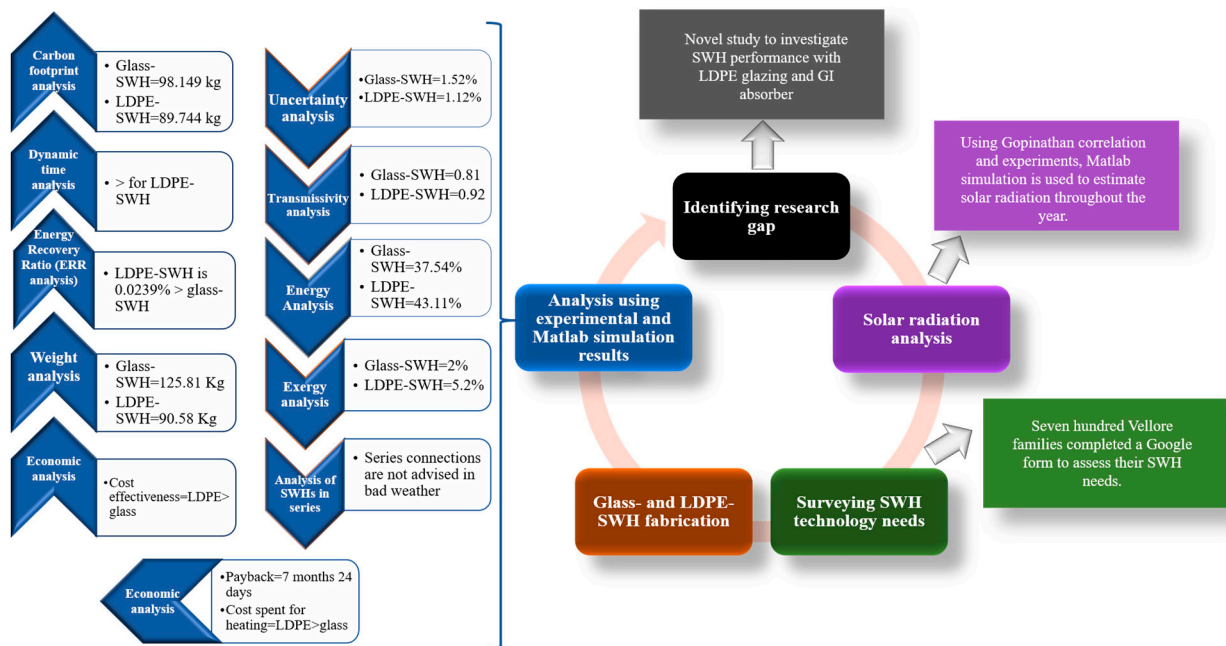


Figure 1. Workflow.

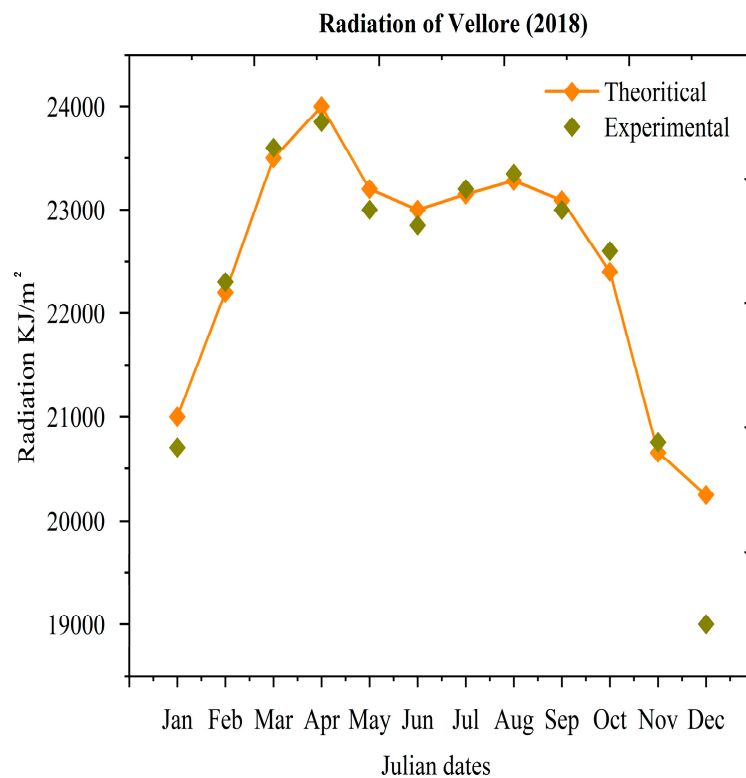


Figure 2. Solar radiation of Vellore (2018).

2.2. Survey

Surveys provide decision-making information. Getting answers to essential questions helps identify ways to improve any system. This survey helps design and build an SWH by revealing the community’s needs. Figure 3 shows the satellite image of Brahmapuram, Vellore (12.957831° N, 79.171664° E), chosen as the location for a Google form survey. Brahmapuram is a village in Vellore’s Katpadi taluk with 8430 people [25]. Seven hundred families participated in a Google form survey with ten questions and three to four options

each, based on end-user needs. The survey questions were designed to cover a wide range of people, where some questions were focused on actual SWH users and some on potential new customers. The survey follows Office of Management and Budget (OMB) standards and guidelines [26]. The poll showed that the public understands solar thermal technologies, and the survey results in Table 1 help design and manufacture SWHs. The glass SWH and LDPE SWH were developed using public feedback.

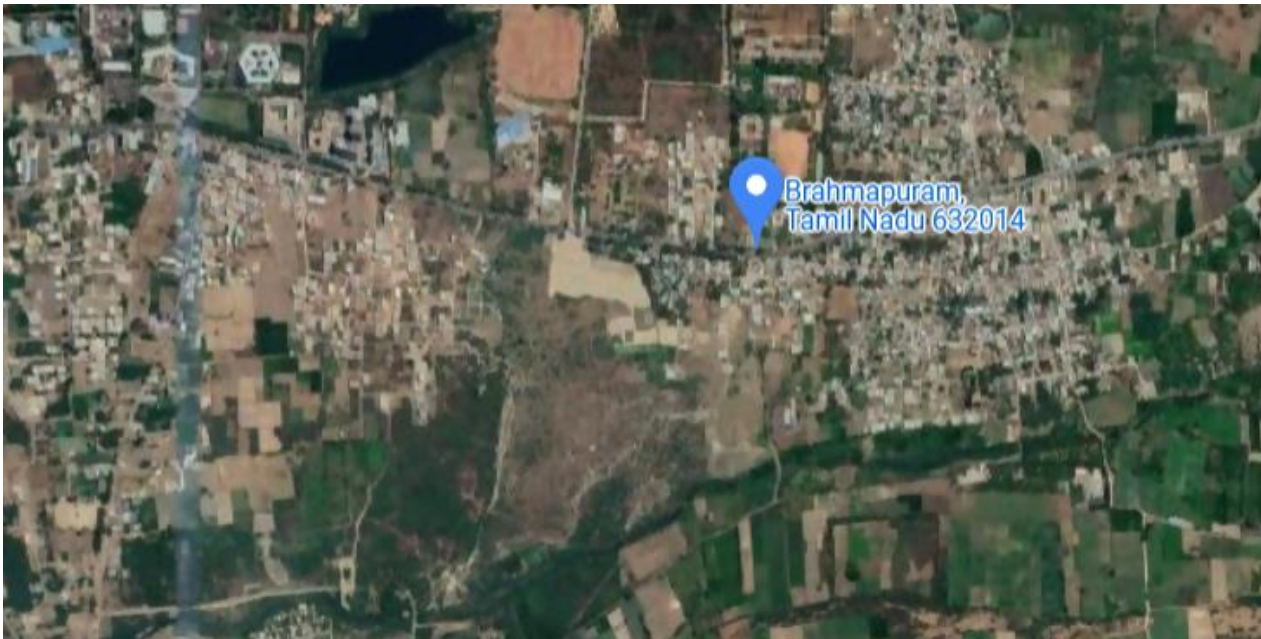


Figure 3. Satellite image of Brahmapuram, Vellore District.

Table 1. Survey results.

Sl. No.	Survey Questions	Survey Results								
1.	Is there any specific climate requirement for working of solar water heater?	<p>Survey Results</p> <table border="1"> <thead> <tr> <th>Climate</th> <th>Percentage</th> </tr> </thead> <tbody> <tr> <td>Summer</td> <td>61.60%</td> </tr> <tr> <td>Winter</td> <td>28.80%</td> </tr> <tr> <td>Rainy</td> <td>9.60%</td> </tr> </tbody> </table> <p>■ Winter ■ Summer ■ Rainy</p>	Climate	Percentage	Summer	61.60%	Winter	28.80%	Rainy	9.60%
Climate	Percentage									
Summer	61.60%									
Winter	28.80%									
Rainy	9.60%									
2.	Does the area have hard water (with soap solutions from less white foam)?	<p>Survey Results</p> <table border="1"> <thead> <tr> <th>Response</th> <th>Percentage</th> </tr> </thead> <tbody> <tr> <td>Yes</td> <td>57.70%</td> </tr> <tr> <td>No</td> <td>42.30%</td> </tr> </tbody> </table> <p>■ Yes ■ No</p>	Response	Percentage	Yes	57.70%	No	42.30%		
Response	Percentage									
Yes	57.70%									
No	42.30%									

Table 1. Cont.

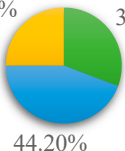
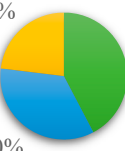
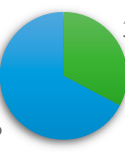
Sl. No.	Survey Questions	Survey Results
3.	What is the required life of the solar water heating system?	<p style="text-align: center;">Survey Results</p>  <p style="text-align: center;">25% 30.80%</p> <p style="text-align: center;">44.20%</p> <p style="text-align: center;">■ 5 Years ■ 10 Years ■ 15 Years</p>
4.	What is the temperature of the hot water required?	<p style="text-align: center;">Survey Results</p>  <p style="text-align: center;">7.70% 9.60%</p> <p style="text-align: center;">82.70%</p> <p style="text-align: center;">■ High (untouchable)</p> <p style="text-align: center;">■ Medium (to be mixed with more amount of water)</p> <p style="text-align: center;">■ Low (touchable and directly used)</p>
5.	Where do you want it to be installed?	<p style="text-align: center;">Survey Results</p>  <p style="text-align: center;">23.10% 42.30%</p> <p style="text-align: center;">34.60%</p> <p style="text-align: center;">■ Building terrace ■ Roof tops</p> <p style="text-align: center;">■ Wall mounting</p>
6.	Do you want it to be common for the whole building or only for your family?	<p style="text-align: center;">Survey Results</p>  <p style="text-align: center;">32.70%</p> <p style="text-align: center;">67.30%</p> <p style="text-align: center;">■ Only for one family</p> <p style="text-align: center;">■ Common for whole family</p>

Table 1. Cont.

Sl. No.	Survey Questions	Survey Results										
7.	What is the type of terrace flooring used?	<p style="text-align: center;">Survey Results</p> <table border="1"> <caption>Survey Results for Question 7</caption> <thead> <tr> <th>Flooring Type</th> <th>Percentage</th> </tr> </thead> <tbody> <tr> <td>Ceramic tiles</td> <td>19.20%</td> </tr> <tr> <td>Brick flooring</td> <td>21.20%</td> </tr> <tr> <td>Concrete flooring</td> <td>59.60%</td> </tr> </tbody> </table>	Flooring Type	Percentage	Ceramic tiles	19.20%	Brick flooring	21.20%	Concrete flooring	59.60%		
Flooring Type	Percentage											
Ceramic tiles	19.20%											
Brick flooring	21.20%											
Concrete flooring	59.60%											
8.	What direction is your residence facing?	<p style="text-align: center;">Survey Results</p> <table border="1"> <caption>Survey Results for Question 8</caption> <thead> <tr> <th>Direction</th> <th>Percentage</th> </tr> </thead> <tbody> <tr> <td>North</td> <td>13.50%</td> </tr> <tr> <td>East</td> <td>25%</td> </tr> <tr> <td>West</td> <td>13.50%</td> </tr> <tr> <td>South</td> <td>48.10%</td> </tr> </tbody> </table>	Direction	Percentage	North	13.50%	East	25%	West	13.50%	South	48.10%
Direction	Percentage											
North	13.50%											
East	25%											
West	13.50%											
South	48.10%											
9.	Which type of water is to be used?	<p style="text-align: center;">Survey Results</p> <table border="1"> <caption>Survey Results for Question 9</caption> <thead> <tr> <th>Water Type</th> <th>Percentage</th> </tr> </thead> <tbody> <tr> <td>Bore well water</td> <td>32.70%</td> </tr> <tr> <td>Municipality treated water</td> <td>34.60%</td> </tr> <tr> <td>Tank water</td> <td>32.70%</td> </tr> </tbody> </table>	Water Type	Percentage	Bore well water	32.70%	Municipality treated water	34.60%	Tank water	32.70%		
Water Type	Percentage											
Bore well water	32.70%											
Municipality treated water	34.60%											
Tank water	32.70%											
10	How many hours are required to heat the water?	<p style="text-align: center;">Survey Results</p> <table border="1"> <caption>Survey Results for Question 10</caption> <thead> <tr> <th>Hours</th> <th>Percentage</th> </tr> </thead> <tbody> <tr> <td>Less than 6 hours</td> <td>57.70%</td> </tr> <tr> <td>6 to 7 hours</td> <td>28.80%</td> </tr> <tr> <td>More than 7 hours</td> <td>13.50%</td> </tr> </tbody> </table>	Hours	Percentage	Less than 6 hours	57.70%	6 to 7 hours	28.80%	More than 7 hours	13.50%		
Hours	Percentage											
Less than 6 hours	57.70%											
6 to 7 hours	28.80%											
More than 7 hours	13.50%											

2.3. Experiment

2.3.1. Thermophysical and Radiometric Characterization

Glass, LDPE transparent cover, galvanized iron (GI) sheets, GI tubes, hardwood sheets, thermocol, glass wool, and necessary fastening supplies for the fabrication of LDPE and glass SWHs were obtained from Hardware & Mill Stores (HMS) in Vellore, India. Thermophysical and radiometric parameters were measured as part of the investigation as they influence heat transport, efficiency, and other aspects. Table 2 shows the specifications of the components used in fabrication. To ensure heirlooms, certain qualities were measured. Thermal conductivity (k) of the absorber plate and insulation materials were determined using the Transient Hot Wire (THW) method with a KD2 pro thermal property analyzer (accuracy: $\pm 5\%$). The absorber plate's absorptivity and emissivity were measured using a single wave spectrometer (Model: LMSP-V325, Das Instruments and Solutions, Chennai, India, Accuracy: $\pm 0.5\%$). Glass and LDPE refractive indices were measured using the V-block method on a KPR300 refractometer (accuracy: $\pm 0.00004\%$). The thickness of the components was measured with a precision meter (Model: 3109-25A, Insize, Ahmedabad, India, Accuracy: $\pm 0.1\%$).

Table 2. Specifications of the components.

Component	Specifications
Absorber plate	Material—Galvanized iron Length—1.8 m Width—1.2 m Thickness—0.0012 m Thermal conductivity—68 W/m-K Absorptivity—0.92 Emissivity—0.23 Space between plate and glazing—0.065 m
HTF pipe	Riser pipes: Material—Galvanized iron Outer diameter—0.01905 m Length—1.8 m The center-to-center distance of Tubes—1.2 m No. of tubes—5 Header and footer pipes: Material—galvanized iron Outer diameter—0.03175 m Length—1.3 m
Glazing	Glass: Thickness—0.004 m Refractive index—1.52 Transmissivity—0.81 LDPE: Thickness—0.00018 m Refractive index—1.49 Transmissivity—0.92
Frame	Material—wood Length—2.2 m Width—1.4 m
Insulation	Material—Thermocol and Glass wool Thickness—0.08 m Thermal conductivity—0.04 W/m-K

2.3.2. Working

Survey results were used to build two SWHs with glass and LDPE glazing. To compensate for the thermal conductivity difference between GI and copper, the collector was built with double the contact area between the riser pipes and the absorber sheet than a typical collector. The inlet pipe was attached to the flat plate collector's side, via which gravity-driven water flow occurs. The absorber plate absorbs heat in both the SWHs. The glass and LDPE cover is opaque to infrared rays and transparent to solar light in the visible range. As a result, it enables the solar radiation to reach the collector. As a result, it will let solar radiation through while blocking the longer wavelength from leaving the collector. The absorber plate will thus capture the most solar radiation directed at it, and the former will transfer it to the working fluid, typically water. Now that the water is heated inside the tube, the water's temperature increases. Because of this, heated water has a lower density than cold water. The hot water emerges from the collector's top due to this density disparity. This idea is known as the "thermosyphon" principle. The hot water is thus gathered at the collector's top while the operation continues.

2.3.3. Experimental Procedure

Figure 4a shows the schematic of the experimental setup. It is made up of a tank (capacity: 100 L, dimensions: 0.925 m height, 0.585 m diameter), a pump (Make: HSN/SAC:84137093 Havells, New Delhi, India, Power: 0.5 HP), a flow sensor (Make: LZM-15T, Jingyig, Ningbo, China, Accuracy: $\pm 4\%$), a pyranometer, a DAQ (Make: Agilent 34970A, Keysight Technologies, Santa Rosa, CA, USA), K-type thermocouples (Accuracy: $\pm 0.5\text{ }^\circ\text{C}$), SWHs, and PC. The SWHs with glass and LDPE glazing were operated simultaneously on 28 March 2018, in Vellore, India, at 5 min intervals. Figure 4b,c depicts the glass SWH and LDPE SWH. For testing, the Ministry of New and Renewable Energy's (MNRE) IS 12933 (part-5):2003 standards were used [27]. Before the experiment, the measurement equipment, water level, water flow rate, leakage, sensor function, and glazing dust were checked. In both SWHs, a pump circulated heat transfer fluid (water) in a closed loop. Throughout the experiment, a flow sensor recorded 0.013 kg/s in both SWHs. The highest and lowest ambient temperatures were $42\text{ }^\circ\text{C}$ and $23\text{ }^\circ\text{C}$. Attached to a DAQ, the thermocouples' data were averaged every 5 min.

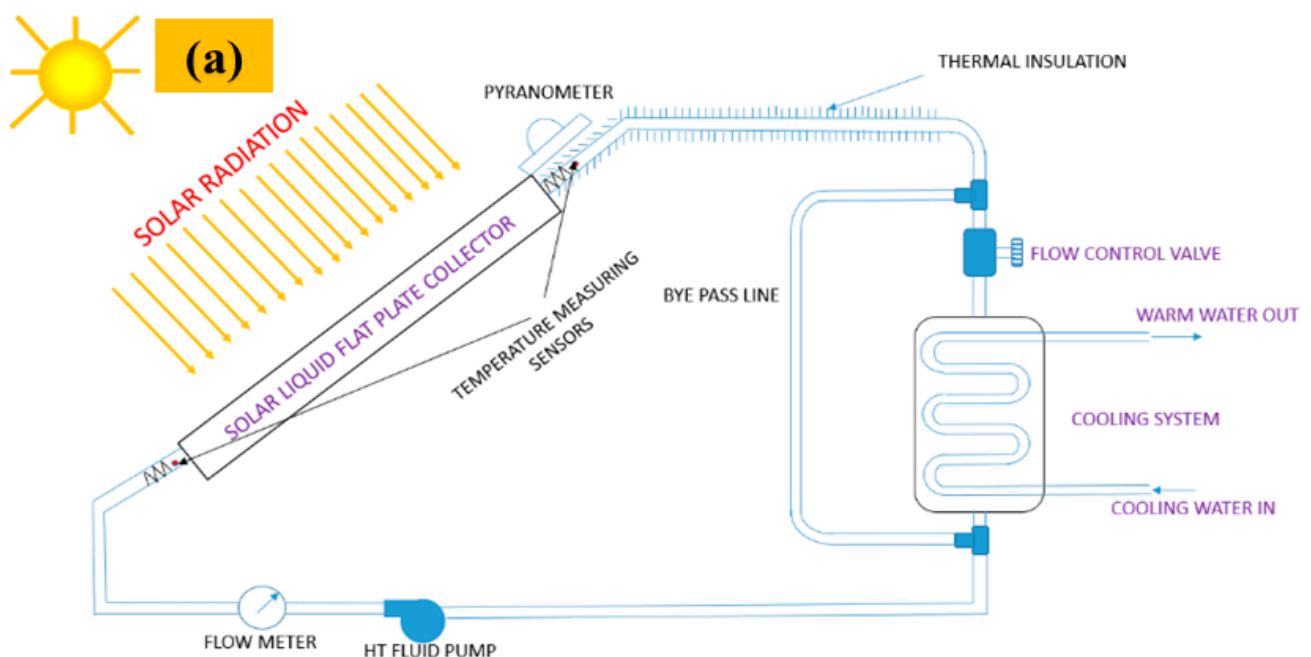


Figure 4. Cont.

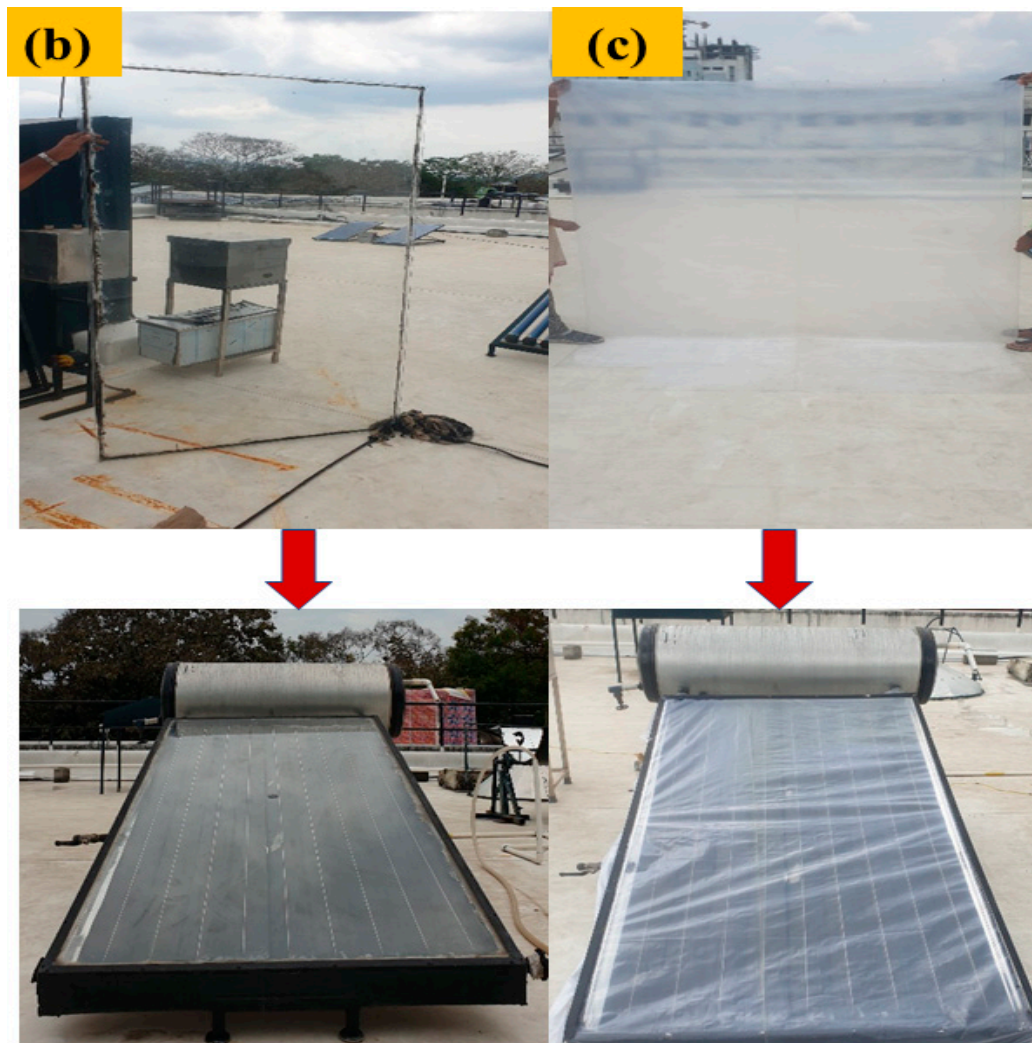


Figure 4. (a) Schematic of the experimental setup. (b) Glass SWH; (c) LDPE SWH.

2.3.4. Energy Efficiency

The total radiation (I_τ) is calculated using [23]

$$I_\tau = I_b T_{bR} + I_d T_{dR} + (I_b + I_d) T_{RR} \quad (2)$$

where, I_τ , I_b , and I_d are total radiation, beam radiation, and diffuse radiation, respectively. T_{bR} is the tilt factor for beam radiation. T_{dR} is the tilt factor for diffuse radiation and T_{RR} is the tilt factor for reflected radiation. The total flux absorbed by the absorber plate (F_a) is estimated by [23]

$$F_a = I_b T_{bR} (\tau\alpha)_b + \{I_d T_{dR} + (I_b + I_d) T_{RR}\} (\tau\alpha)_d \quad (3)$$

where $(\tau\alpha)_b$ and $(\tau\alpha)_d$ are transmissivity constants of the absorber plate in case of the beam and diffuse radiation. The instantaneous efficiency (η_i) of the collector is calculated using

$$\eta_i = \frac{Q_U}{A_c I_\tau} \quad (4)$$

where η_i is collector efficiency, Q_U is useful for heat gain ($Q_U = \dot{m} C_{PS} \Delta T$) [23], and A_c is the collector area.

2.3.5. Exergy Efficiency

Exergy is a system's maximum steady-state work derived from the second law of thermodynamics [28]. Entropy measures unpredictability and irrepressibility. As system irreversibility increases, so do entropy and exergy. The exergy efficiency is calculated using the following exergy equations [29,30].

$$\mathcal{E}x_{heat} - \mathcal{E}x_{work} - \mathcal{E}x_{mass, in} - \mathcal{E}x_{mass, out} = \mathcal{E}x_{dest} \quad (5)$$

where $\mathcal{E}x_{dest}$ is exergy destruction, $\mathcal{E}x_{heat}$ is exergy in heat, $\mathcal{E}x_{work}$ is exergy in work, $\mathcal{E}x_{mass, in}$ is exergy in the mass inlet, and $\mathcal{E}x_{mass, out}$ is exergy in the mass outlet. By substitution and simplification, the exergy destruction equation becomes

$$\sum (1 - T_a/T_{surf})q_s - [\dot{m}(h_o - h_i) - T_a(S_o - S_i)] = \mathcal{E}x_{dest} \quad (6)$$

where T_a is the ambient temperature, T_{surf} is the surface temperature of the sun, q_s is the available energy from solar radiation, h_o and h_i are enthalpy out and enthalpy in, and S_o and S_i are entropy out and entropy in [25]. The entropy generation is expressed by

$$\dot{\mathcal{E}}_{gen} = \dot{m}C_{PS} \ln(T_{out}/T_{in}) - (q_s/T_{surf}) + (q_o/T_a) \quad (7)$$

where $\dot{\mathcal{E}}_{gen}$ is entropy generation, C_{PS} is the specific heat enthalpy of HTF used, T_{out} and T_{in} are the outlet and inlet temperatures, and q_o is the heat loss. The exergy efficiency compares the solar water heating system's actual output to its reversible output given by the expression.

$$\eta_{\mathcal{E}} = 1 - T_a \dot{\mathcal{E}}_{gen} / \left[1 - (T_a/T_{surf})q_s \right] \quad (8)$$

where $\eta_{\mathcal{E}}$ is exergy efficiency.

2.3.6. Transmissivity

Transmissivity refers to the amount of light energy that passes through a transparent medium. The transmissivity of glass (thickness: 4 mm) and an LDPE (thickness: 0.18 mm) transparent cover with one square foot dimensions were tested experimentally. Both glazings were upheld on a sunny afternoon (27 March 2018), when the maximum radiation was 752 W/m^2 and radiation falling on the surface (I_S) and radiation on the other side (I_B) after passing through glazing were measured using a pyranometer and a DAQ. The transmissivity of glass and LDPE is calculated using the formula [23]

$$\check{T} = \frac{I_B}{I_S} \quad (9)$$

By considering reflection-refraction and absorption separately, a collector's cover system transmissivity can be calculated accurately by following equations using MATLAB R2020a [23].

$$\check{T} = \tau_r \tau_a \quad (10)$$

where τ_r is the transmissivity by considering reflection and refraction and τ_a is the transmissivity by considering absorption.

$$\tau_r = 1/2 (t_{\uparrow} t_{\downarrow}) \quad (11)$$

where t_{\uparrow} and t_{\downarrow} are two components of polarization.

$$\tau_a = e^{-\kappa g} \quad (12)$$

where κ is the extinction coefficient and g is the thickness of the cover.

2.3.7. Uncertainty

Uncertainty analysis, or experimental error evaluation, is crucial for accurate experiment data [31]. The equation gives the uncertainty analysis general equation

$$U_t^2 = \sum_{i=1}^n U_{ti}^2 \quad (13)$$

where U_t is the uncertainty of the whole experimentation and U_{ti} is the sum of uncertainties of individual parameters.

$$U_{ti} = \eta_i \times \sqrt{\left(\frac{U_r}{\dot{m}}\right)^2} + \sqrt{\left(\frac{U_{q_s}}{q_s}\right)^2} + \sqrt{\left(\frac{U_T}{T_{in}}\right)^2} + \sqrt{\left(\frac{U_T}{T_{out}}\right)^2} + \sqrt{\left(\frac{U_T}{T_a}\right)^2} \quad (14)$$

where U_r is the uncertainty of the roto meter (acrylic panel water flow meter), whose range is 0–400 L/Hr and error value is ± 0.5 L/Hr, which measures the mass flow rate of HTF. U_{q_s} is the uncertainty of the pyranometer, whose range and error reading is 0–4000 W/m² and ± 1 W/m², which measures the total solar radiation available. U_T is the uncertainty of K-type thermocouple wire (Ni-Cr type) with a range of 0–200 °C and error reading of ± 0.5 °C, which measures the ambient temperature, outlet, and inlet temperatures of the HTF. The uncertainty values of individual parameters are shown in Table 3 as uncertainty results. During glass and LDPE transparent cover experiments, the collector's overall uncertainty was 1.52% and 1.12%. Experiments were repeated to compare data variations with standard simulated values. Measuring accuracy was increased to reduce uncertainty and obtain the FPSWH's desired results.

Table 3. Uncertainty results.

Parameter	Uncertainty in Glass Cover Experiment	Uncertainty in the Transparent Cover Experiment
Flow rate	0.2%	0.17%
Temperature difference	0.59%	0.35%

2.3.8. Payback Period

The payback period calculated in economic analysis estimates when an energy investment will pay off. Table 4 shows capital cost estimation. Comparing the SWH to a 2 kWh electric geyser yields annual net savings. The SWH's payback period can be calculated using [32]

$$P = C_A / A_S \quad (15)$$

where P is the payback period, C_A is capital cost, and A_S is annual net savings.

Table 4. Capital cost estimation.

Description	Quantity	Cost (Rupees)
G.I Riser pipes	5 nos.	850
G.I header and footer pipes	2 nos.	350
G.I absorber sheet	1 no.	1550
Welding	-	600
Solar Paint	1 no.	500
Wooden box	1 no.	1250
Insulation	-	600
Glass Plate	1	1150
LDPE transparent cover	-	500
Storage tank	1	2000

Table 4. *Cont.*

Description	Quantity	Cost (Rupees)
Other expenses	-	700
Total	-	10,050

2.3.9. CO₂ Emissions

When using coal as an energy source, the average carbon dioxide (CO₂) intensity is 0.98 kg of CO₂ per kWh. The value 0.98 becomes 1.58 if the loss of transportation and distribution is 40% and the loss of domestic devices is about 20%. As a result, the typical CO₂ intensity for fossil fuel power plants is 1.58 kg of CO₂ per kWh [33].

$$\text{Annual CO}_2 \text{ emissions (Kg/y)} = (\dot{E}_t \times 1.58) / \dot{L}T \quad (16)$$

where \dot{E}_t is the embodied energy and $\dot{L}T$ is the lifetime of SWHs (assumed to be 25 years) [34].

$$\text{Lifetime CO}_2 \text{ mitigation} = \dot{E}oe \times 1.58 \times \dot{L}T \quad (17)$$

where $\dot{E}oe$ is the annual energy output in terms of exergy.

$$\dot{E}ot = \text{Annual average radiation (kWh)} \times \text{SWH efficiency} \quad (18)$$

where $\dot{E}ot$ is the thermal energy output.

$$\dot{E}oe = \dot{E}ot \times \left[1 + \left(\frac{25 + 273}{T + 273} \right) \right] \quad (19)$$

where T is the SWH's operating temperature [35].

$$\text{Net CO}_2 \text{ mitigation} = \frac{\left((\dot{E}oe \times \dot{L}T) - \dot{E}_t \right) \times 1.58}{1000} \quad (20)$$

$$\text{Carbon credit earned} = \text{Net CO}_2 \text{ mitigation} \times \text{CO}_2 \text{ cost per ton} \quad (21)$$

3. Results and Discussion

3.1. Solar Transmissivity Analysis

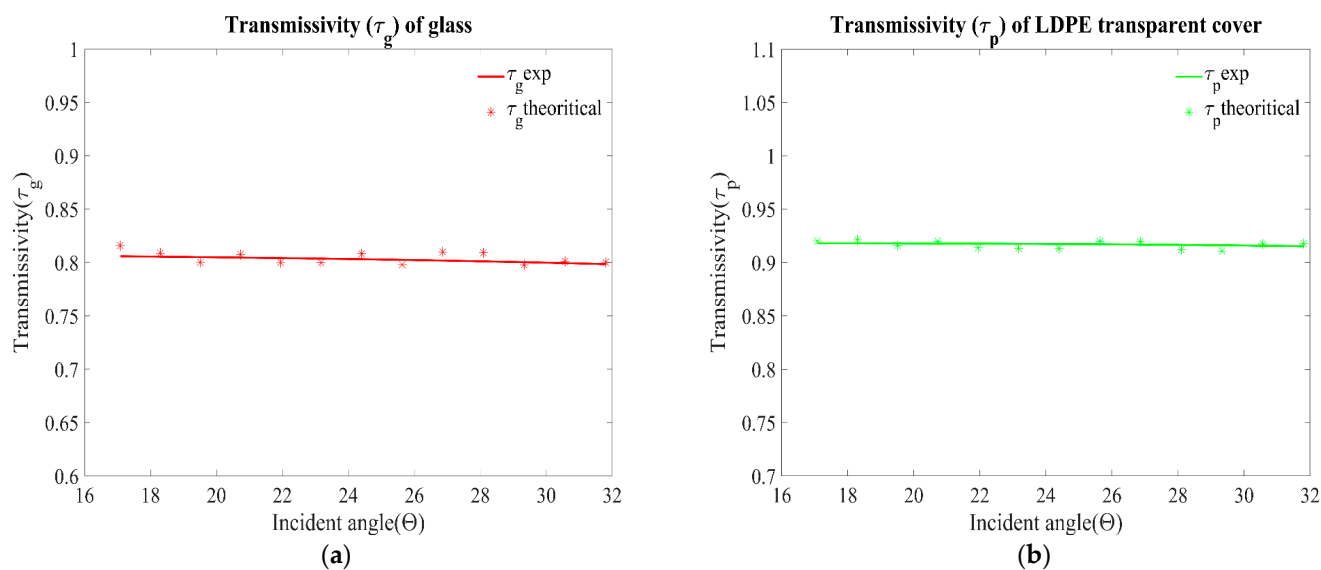
Most polymers today are polyolefins. They are classified into two types, polyethylene and polypropylene, based on temperature and chemical resistance, density, flexibility, and other factors. Our application is glazing-oriented, so we use polyethylene. Linear low-density polyethylene (LLDPE), low-density polyethylene (LDPE), medium-density polyethylene (MDPE), and high-density polyethylene (HDPE) all have increasing crystallinity as density increases. Specific heat is directly proportional to crystallinity, and conductivity is inversely proportional to crystallinity [36]. Specific heat capacity (C_p) is the energy needed per unit mass to raise or lower temperatures by 1 °C [37]. Thermal conductivity (k) measures heat transfer [38]. Materials with high thermal conductivity are preferred when thermal energy must be delivered to an absorber through glazing. Structure determines the thermal conductivity of a material. In metals, free electrons transport heat. Non-metallic polymers transport heat via phonons. Density increases polyethylene crystallinity, but crystallinity decreases heat conductivity [39]. Therefore, we use LDPE, which has the lowest density and crystallinity. Table 5 shows polyethylene properties. In transmissivity, polyethylene outperforms polyvinyl chloride, polystyrene, and polycarbonate [40].

Table 5. Polyethylene properties.

	LLDPE	LDPE	MDPE	HDPE
Name	Linear low-density polyethylene	Low-density polyethylene	Medium-density polyethylene	High-density polyethylene
Density	0.922 g/cm ³	0.918 g/cm ³	0.935 g/cm ³	0.954 g/cm ³
Crystallinity	39.45% Semi-crystalline	38.73% Low crystalline and high amorphous	48.36% Medium crystalline and amorphous	51.17% High crystalline and amorphous

When choosing a collector glazing material, the solar wavelength transmissivity coefficient should be considered. ISO 9050:2003 [41] (glasses in buildings) regulates solar transmittance as an index of perpendicularly incident solar energy transmitted by transparent materials. The higher the solar transmissivity coefficient, the hotter the air between the glazing and the absorber. The glazing is always mostly glass. Glass's high solar transmissivity and low Low Wave Infrared (LWIR) transmissivity make it a popular collector glazing. Low LWIR transmissivity reduces collection region radiation transmission. LDPE covers are a new glass alternative. LDPE with a solar transmissivity coefficient equal to or greater than glass can increase transmitted light, but the literature on LDPE solar transmittance and LDPE glazing in SWHs is scarce. This is due to LDPE's strong LWIR transmissivity coefficient. LDPE was therefore replaced by polyethylene-co-vinyl acetate (EVA) and then by ethylene-tetrafluoroethylene copolymer (ETFE) [18].

LDPE is less expensive and requires a lighter, cheaper support structure than glass and other plastic fiber glazings. LDPE is resistant to chemicals and microbes and has good mechanical and thermo-optical qualities. Solar radiation, high ambient temperature, relative humidity, wind, and other factors reduce LDPE's useful life, but thickness and additives determine its lifespan [18]. When an SWH with a small absorber area is covered with LDPE, its strong LWIR transmittance is irrelevant. SWHs with glass and LDPE transparent cover glazing were tested. The solar transmissivity coefficients of glass and LDPE were measured and compared using MATLAB R2022a. Figure 5a,b shows the transmissivity of glass and LDPE, respectively. Figure 6 shows the flow chart of the transmissivity analysis simulation program. The solar water heater had an inclined surface facing due south, a thickness of 4 mm for glass and 0.180 mm for LDPE, and refractive indices of 1.52 and 1.49, with extinction coefficients of 32 m and 632.8 nm, respectively. LDPE's solar transmissivity coefficient is equal to or better than glass, so it can be used as a glazing material in SWHs to save money and weight without sacrificing efficiency.

**Figure 5.** (a) Transmissivity of glass; (b) transmissivity of LDPE.

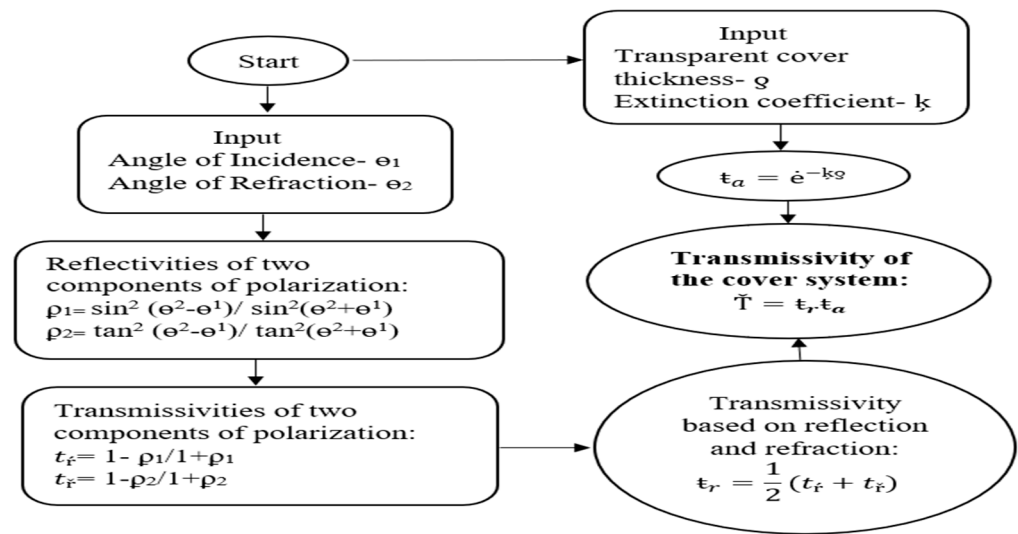


Figure 6. Flow chart of transmissivity analysis simulation program.

3.2. Energy Analysis

SWHs produce water at desired temperatures. Thus, SWH outlet water temperature matters. A resource efficiency study shows how to achieve the desired outlet water temperature [42]. In Figure 7a,b, the output water temperature and efficiency of both SWHs (with glass and LDPE glazing) are compared with numerically assessed data. The numerical evaluation of both SWHs is performed with MATLAB R2022a. The following assumptions were made for numerical assessments: (1) Absorber plate heat transfer is steady-state. (2) HTF tube pressure drop is ignored [43]. Figure 8 shows the flow chart of the simulation program. Experimental and numerical data are nearly identical. As more beneficial radiation is available, HTF exit temperature may rise. The outlet temperature rises directly with radiation as noon approaches. Glass and LDPE SWHs have maximum outlet water temperatures of 54.4 °C and 74.6 °C, respectively. The difference between theoretical and experimental output water temperature is 0.6 °C in a glass-covered SWH and 1.6 °C in an LDPE-covered SWH. Both SWHs achieve 37.54% and 43.11% experimental efficiency, which matches the theoretical data. Figure 7b shows a gradual decrease in efficiency due to cloudy skies on the experimental day. The transparent cover improved efficiency by 5.57% at midday.

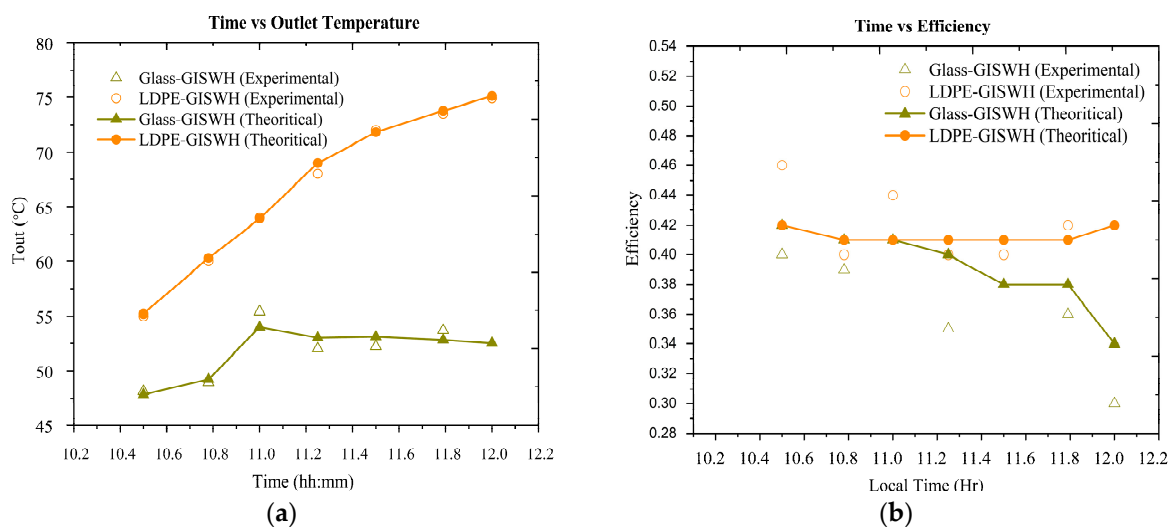


Figure 7. (a) Outlet temperature; (b) efficiency.

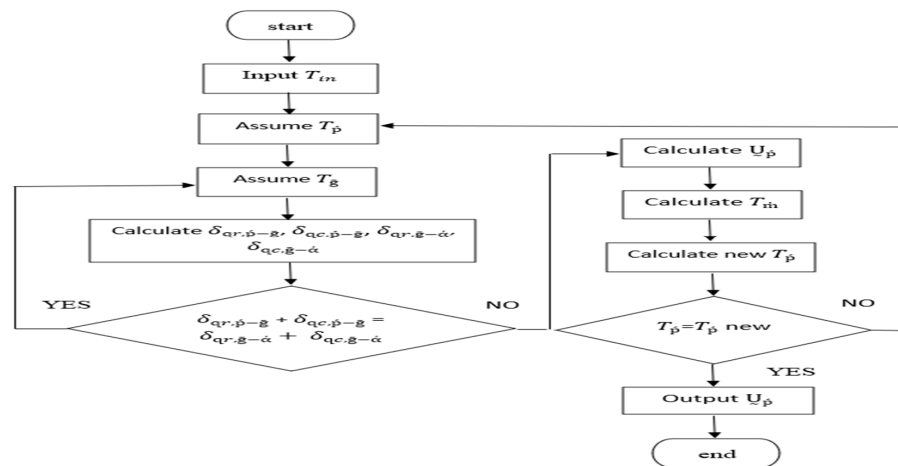


Figure 8. Flow chart of the simulation program.

3.3. Series Connection of Fabricated Solar Water Heaters

Sequencing SWHs raises outlet fluid temperature more than paralleling them [44]. As the constructed SWH lacks a storage tank, an experimental-simulated series analysis is performed to obtain the required temperature during inclement weather. Three solar water heaters are studied in series (with glass and LDPE glazing). MATLAB R2020a determines the series SWH system and the mount configuration effect on outlet water temperature. It is assumed that SWHs are connected in series one after the other, and simulation is performed for two conditions as follows: (1) Simulation for the second and third SWHs alone from 10 a.m. to 12 p.m. The experimental outlet water temperature values (measured on 28 March 2018) are fed into the second SWH. (2) A simulation based on changing radiation that predicts the ambient water temperature from 6 am to 12 pm and assumes that it is the inlet water for the series system. Figure 9 shows the simulative analysis of glass and LDPE SWHs in series. The investigation found that from 6 to 7:30 a.m., less than 200 W of radiation is needed to reach the target temperature. A series of connections and intense radiation from 10 a.m. to 1 a.m. can achieve desired temperatures. In low insolation and bad weather, series collectors cannot be used as a countermeasure. Therefore, a morning series connection is not recommended for both built SWHs (with glass and LDPE glazing). Future studies will examine using a serpentine flow field pattern in an absorber tube during severe weather.

Outlet Water Temperature of Solar Water Heaters in series

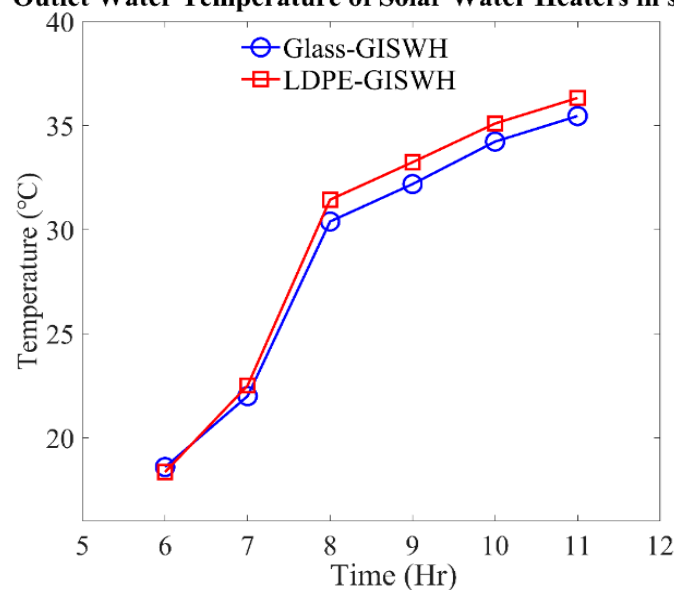


Figure 9. Simulative analysis of solar water heaters in series.

3.4. Exergy Analysis

Irreversible thermal losses increase entropy and reduce efficiency [31]. Exergy analysis includes energy destruction and entropy. Exergy destruction in the SWHs is depicted in Figure 10a. Compared to glass, LDPE reduces exergy loss. Figure 10b shows the exergy efficiency of the SWHs. Entropy generation equals exergy efficiency because exergy efficiency equals destruction. Because an LDPE SWH generates less entropy than a glass SWH, its exergy efficiency is higher. In both cases, as the input-to-output HTF temperature differential increases, so does exergy efficiency. This shows that when the HTF intake and output temperatures differ more, the SWH works efficiently, minimizing exergy losses. An LDPE SWH is 3.2% more efficient than glass.

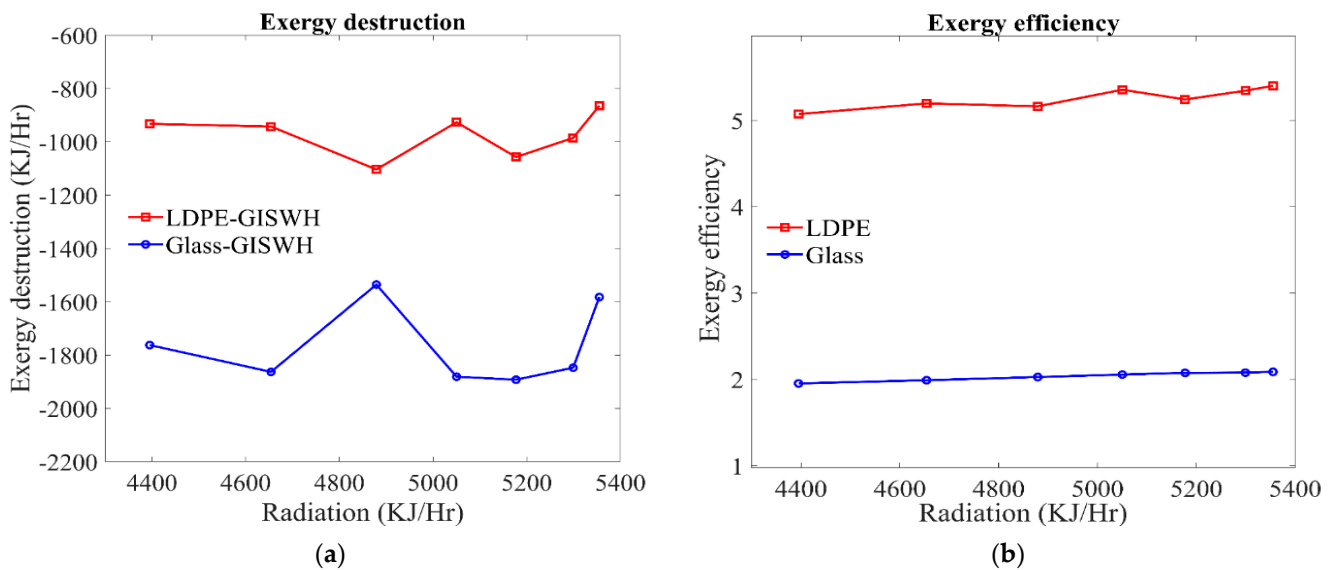


Figure 10. (a) Exergy destruction; (b) exergy efficiency.

3.5. Economic Analysis

3.5.1. Payback Period

The economic analysis calculated a 7-month-and-24-day payback period. After 7 months and 24 days, the SWH investment will be fully recovered. The FPSWH will be free after the payback period.

3.5.2. Cost Spent Based on Power Rating

Both SWHs achieve cost savings in terms of electricity. Our SWHs were cost-effectively compared to a traditional 2 kW electrical geyser [45]. Figure 11a shows the average sun radiation of Vellore from 6 to 10 a.m. every month in 2018. Maximum solar radiation is measured between 6 and 10 a.m. in March and November. September and October have a peak and trough. An overcast sky may cause this difference. Figure 11b shows the cost spent by an SWH v/s electrical geyser in rising water temperature up to 50 °C every day in 2018. A 2 kW electric geyser costs INR 3/day to run annually. In March, April, and May, glass SWHs spent a maximum of INR 2.79 per day and a minimum of INR 2.275. An LDPE SHW spends a maximum of INR 4.47 in January, April, May, October, and December and a minimum of INR 4.455 in the remaining months. It saves INR 0.725 per day versus an electric geyser. The time required to heat water to 50 °C correlates to solar radiation, but the cost cannot be based on one parameter because more radiation may result in less operating time and vice versa. The expense incurred by SWHs in each month of 2018 was calculated from the cost spent on each day. An LDPE SWH spends INR 138.57 to INR 124.74 per month. A glass SWH costs INR 86.49 to INR 63.7.

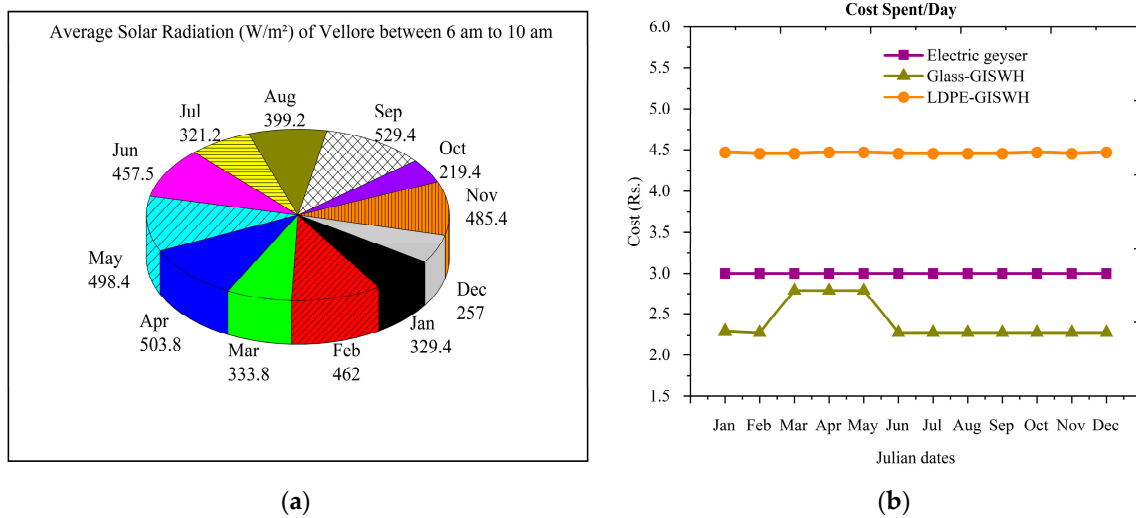


Figure 11. (a) Average solar radiation of Vellore from 6 a.m. to 10 a.m. every month in 2018. (b) Cost spent by an SWH v/s electrical geyser in rising water temp. up to 50 °C every day in 2018.

3.5.3. Cost-Effectiveness

A refurbished SWH with glass glazing costs INR 9550, but with an LDPE clear cover, it costs INR 8900. Tamil Nadu provides a 40% subsidy [46] for the purchase of SWHs in rural areas, reducing investment costs. Compared to a 100 L electric geyser, fabrication costs are lower. LDPE and glass SWHs save INR 13,100 and INR 12,450 by replacing an electric geyser. By installing revitalized LDPE SWHs in 700 Brahmapuram, Vellore families can save INR 9,170,000.

3.6. Weight Reduction on Proposed Model

Low-density polyethylene (LDPE) instead of glass reduced the SWH’s weight. The SWH weighs 125.81 kg with a 37.5 kg glass cover and 90.58 kg with a 2.24 kg transparent cover. By replacing with LDPE, SWH handling and positioning improved by 32.56%.

3.7. ERR Analysis

The AHRI efficiency recovery ratio (ERR) is the ratio of available energy to energy used [47]. ERR compares energy recovery and efficiency of devices. End-user energy savings increase with ERR. Figure 12 shows the efficiency recovery ratio of glass SWHs and LDPE SWHs, where a linear ERR curve for both SWHs is displayed as an ERR proportional to solar radiation. An SWH with LDPE has a 0.0239% higher efficiency recovery ratio than with a glass cover. LDPE glazing has a higher ERR than glass glazing.

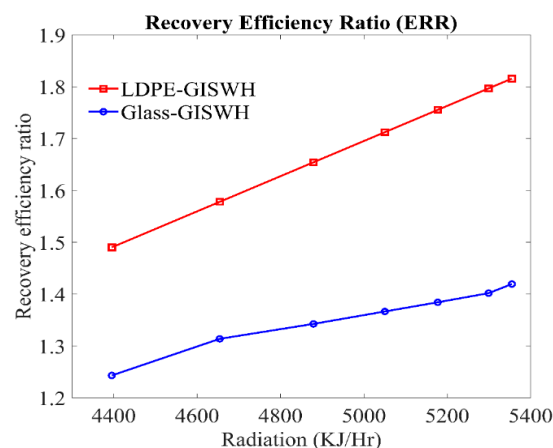


Figure 12. ERR of glass SWHs and LDPE SWHs.

3.8. Dynamic Time Analysis

The dynamic time of a thermal energy recovery system is how long it will take to complete the daily load based on monthly global radiation. Daily and monthly dynamic time forecasts show when the thermal device should operate. Our SWHs' dynamic times were similar after analysis. The average monthly dynamic time is an SWH's time to heat the water to 50 °C. A poll found that most homes bathe with hot water. Therefore, dynamic time was calculated using the average radiation values from 6 to 10 a.m. each month. March and December had the most radiation in 2018. Because solar radiation varies by month, season, and time of day, dynamic time correlates to incident radiation. In September, dynamic time is the lowest, and in October, it is the highest. September's fastest time was 1:35. Figure 13 shows the dynamic time to raise the water temperature to 50 °C.

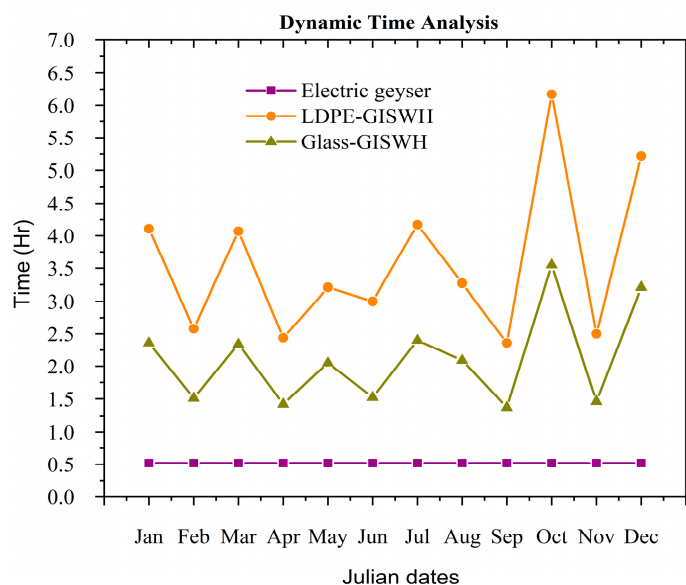


Figure 13. Dynamic time needed to raise the water temperature to 50 °C.

3.9. CO₂ Analysis

Embodied energy represents the energy needed to create goods, services, or other things [48]. Table 6 displays the coefficient of embodied energy for the different materials utilized in SWH production. Manufacturing glass and LDPE SWHs required an estimated total embodied energy of 1553.4 kWh and 1419.7 kWh, respectively. For glass and LDPE SWHs, the CO₂ emission was calculated to be 98.149 kg and 89.744 kg, respectively. Since less energy is needed to replace system components with longer lifespans, the CO₂ emission decreases as the SWH's lifetime increases. Table 7 shows the CO₂ analysis results of glass and LDPE SWHs' carbon emission, mitigation, and carbon credits earned. Compared to an LDPE SWH, which is 2.53 tons and 2.2 tons, a glass SWH provides a larger CO₂ mitigation. As the average solar radiation available in a region increases, so does CO₂ mitigation. Currently, the cost of CO₂ mitigation is projected to be around INR 1644.95 (USD 20 per ton). As a result, the annual carbon credit received by the glass and LDPE SWHs is significant at INR 125.02 (USD 1.52) and INR 419.46 (USD 5.1), respectively.

Table 6. Coefficient of embodied energy [49–52].

Material	Embodied Energy Coefficient (kWh/kg)
GI (absorber and pipe)	9.72
Glass	7.28
LDPE	2.14
Paint	27.25

Table 6. Cont.

Material	Embodied Energy Coefficient (kWh/kg)
Fittings	47.99
Glass wool	2.89

Table 7. CO₂ analysis results.

CO ₂ Emission, CO ₂ Mitigation, Net CO ₂ Mitigation and Carbon Credit Earned				
Cases				
	CO ₂ Emission (kg)	CO ₂ Mitigation (ton)	Net CO ₂ Mitigation (ton)	Carbon Credit Earned (Rupees)
Glass SWH	98.149	2.53	0.076	125.02
LDPE SWH	89.744	2.2	0.225	419.46

4. Conclusions

This paper presents the results of an extensive experimental simulation study to determine which glazing material (LDPE or glass) with GI as an absorber is best suited for water heating. To reduce errors, the experiment is run in parallel in two SWHs under the same outside ambient conditions and with the same measuring instruments. Similarly, MATLAB R2020a is used for the simulation, with common assumptions applied to both scenarios. A poll conducted in Brahmapuram, Vellore, revealed that people are fully aware of modern renewable technology and clearly understand their needs. Two SWHs were designed and built using survey data as input.

1. During the experiment, the uncertainty difference between the SWHs was 0.4%. The solar transmissivity study shows that LDPE has a higher transmissivity coefficient than glass. The typical experimental and quantitatively calculated solar transmissivity coefficient values for LDPE and glass were around 0.92 and 0.81, respectively.
2. The energy and exergy efficiencies of LDPE SWHs were found to be higher than those of glass SWHs, which can be explained by the solar transmissivity coefficient of LDPE being 12.71% higher than that of glass, which increases the temperature difference between the inlet and outlet of the LDPE SWH.
3. For LDPE SWHs and glass SWHs, the highest average energy efficiency was 43.11% and 37.54%, respectively, and the highest average exergy efficiency was 5.1% and 2%.
4. From 6 to 10 am, the simulation's highest average outlet temperature was 33 °C for LDPE and 31 °C for glass SWHs. In bad weather, series connections are not recommended.
5. The economic analysis was performed, and the payback period was calculated as 7 months and 24 days. The most and the least amount spent by LDPE SWHs for energy conversion is INR 138.57 and INR 124.74, respectively, while glass SWHs spent INR 86.49 and INR 63.7. LDPE SWHs cost more, which can be explained by the fact that LDPE has a longer dynamic duration than glass. According to a cost-effectiveness study, installing revitalized LDPE SWHs can save INR 9,170,000 in the 700 family members that participated in the survey from Brahmapuram, Vellore.
6. LDPE glazing reduces SWH weight by 32.56%, improving handling and positioning.
7. LDPE SWHs' efficiency recovery ratio (ERR) is 0.0239% higher than that of glass SWHs.
8. The dynamic time to raise the water temperature to 50 °C is longer for an LDPE SWH, taking up to six hours in October and as little as two hours in September.
9. The total embodied energy required to create glass and LDPE SWHs was estimated to be 1553.4 kWh and 1419.7 kWh, respectively. The CO₂ emissions from glass and LDPE SWHs were calculated to be 98.149 kg and 89.744 kg, respectively. A glass SWH has a bigger CO₂ mitigation than an LDPE SWH, which is 2.53 tons and 2.2 tons. Glass and LDPE SWHs obtain large annual carbon credits valued at INR 125.02 (USD 1.52) and INR 419.46 (USD 5.1), respectively.

Author Contributions: B.D.: data curation, investigation, and writing—original draft; N.M.: conceptualization, methodology, and supervision; S.S.: conceptualization, investigation, methodology, formal analysis, writing—original draft, and supervision; writing—review and editing, investigation, validation, review, and editing; E.C.: conceptualization, investigation, and supervision; writing—review and editing, and investigation; A.B.O.: methodology, formal analysis, software, visualization roles, writing—original draft, and resources; H.X.L.: investigation, methodology, project administration, and resources; and M.K.: investigation, methodology, project administration, and resources. All authors have read and agreed to the published version of the manuscript.

Funding: The work was supported by the Renewable Energy Sources Lab (RES) of the School of Mechanical Engineering, Vellore Institute of Technology, Vellore.

Data Availability Statement: Not applicable.

Conflicts of Interest: The authors declare no conflict of interest.

Abbreviations

Abbreviation	
EPA	Environmental Protection Agency
FPSWH	Flat plate solar water heater
GI	Galvanized iron
glass SWH	glass solar water heater
HTF	Heat transfer fluid
LDPE	Low-density polyethylene
LDPE SWH	Low-density polyethylene solar water heater
ERR	Efficiency Recovery ratio
SWH	Solar water heater
Nomenclature	
A_c	Collector area (m^2)
A_S	Annual net savings
C_A	Capital cost
C_{PS}	Specific heat enthalpy of the HTF used ($J/(Kg \text{ } ^\circ C)$)
\dot{E}_l	Embodied energy
\dot{E}_{gen}	Entropy generation
\dot{E}_{oe}	Annual energy output in terms of exergy
\dot{E}_{ot}	Thermal energy output
F_a	Flux absorbed by absorber plate (W/m^2)
h_o, h_i	Enthalpy out and Enthalpy in
I_b	Beam radiation (W/m^2)
I_d	Diffuse radiation (W/m^2)
I_τ	Total radiation (W/m^2)
K	Extinction coefficient
$\dot{L}T$	Lifetime of SWH
\dot{m}	Mass flux (kg/s)
P	Payback period
g	Thickness of the cover
q_o	Heat loss (W)
q_s	Available energy from solar radiation (W)
Q_U	Useful heat gain (W)
S_o, S_i	Entropy out and Entropy in
\check{T}	Transmissivity
T_a	Ambient temperature (K)
\check{t}_a	Transmissivity by considering absorption
\check{t}_r	Transmissivity by considering reflection and refraction
t_f, t_r	Two components of polarization
T_{bR}	Tilt factor for beam radiation
T_{dR}	Tilt factor for diffuse radiation
T_g	Average temperature of glazing (K)
T_m	Average temperature of metal tube (K)

T_{out}, T_{in}	Outlet and Inlet temperature of HTF used (K)
T_p	Average absorber plate temperature (K)
T_{RR}	Tilt factor for reflected radiation
T_{surf}	Surface temperature of sun
U_p	Heat loss coefficient of absorber plate
U_r	Uncertainty of rotameter
U_t	Uncertainty of the whole experimentation
U_T	Uncertainty of K-type thermocouple wire
U_{ti}	Sum of uncertainties of individual parameters
U_{qs}	Uncertainty of pyranometer
Greek Letters	
$\mathcal{E}x_{dest}$	Exergy destruction
$\mathcal{E}x_{heat}$	Exergy in available radiation
$\mathcal{E}x_{mass, in}$	Exergy in mass inlet
$\mathcal{E}x_{mass, out}$	Exergy in mass outlet
$\delta_{qc, \bar{g}-\dot{\alpha}}$	Convective heat transfer from glazing to environment
$\delta_{qc, \dot{p}-\bar{g}}$	Convective heat transfer from absorber plate to glazing
$\delta_{qr, \bar{g}-\dot{\alpha}}$	Radiative heat transfer from glazing to environment
$\delta_{qr, \dot{p}-\bar{g}}$	Radiative heat transfer from absorber plate to glazing
η_i	Collector efficiency
η_ε	Exergy efficiency
$(\tau\alpha)_b, (\tau\alpha)_d$	Transmissivity constants of absorber plate in case of beam and diffuse radiation

References

- Li, J.; Huang, J. The expansion of China's solar energy: Challenges and policy options. *Renew. Sustain. Energy Rev.* **2020**, *132*, 110002. [\[CrossRef\]](#)
- Eltaweel, M.; Abdel-Rehim, A.A. Energy and exergy analysis of a thermosiphon and forced-circulation flat-plate solar collector using MWCNT/Water nanofluid. *Case Stud. Therm. Eng.* **2019**, *14*, 100416. [\[CrossRef\]](#)
- Sint, N.K.C.; Choudhury, I.; Masjuki, H.; Aoyama, H. Theoretical analysis to determine the efficiency of a CuO-water nanofluid based-flat plate solar collector for domestic solar water heating system in Myanmar. *Sol. Energy* **2017**, *155*, 608–619. [\[CrossRef\]](#)
- Kohol , Y.W.; Fohagui, F.C.V.; Tchien, G. Flat-plate solar collector thermal performance assessment via energy, exergy and irreversibility analysis. *Energy Convers. Manag. X* **2022**, *15*, 100247. [\[CrossRef\]](#)
- Chen, B.-R.; Chang, Y.-W.; Lee, W.-S.; Chen, S.-L. Long-term thermal performance of a two-phase thermosiphon solar water heater. *Sol. Energy* **2009**, *83*, 1048–1055. [\[CrossRef\]](#)
- Baruah, E.; Konwar, P. Design of a Solar Flat Plate Collector. 2017. Available online: www.ijlera.com (accessed on 27 July 2020).
- Kundu, B. Performance analysis and optimization of absorber plates of different geometry for a flat-plate solar collector: A comparative study. *Appl. Therm. Eng.* **2002**, *22*, 999–1012. [\[CrossRef\]](#)
- Natarajan, E.; Sathish, R. Role of nanofluids in solar water heater. *Int. J. Adv. Manuf. Technol.* **2009**, *45*, 1–5. [\[CrossRef\]](#)
- Kumar, A. Investigation of twisted tape inserted solar water heaters—Heat transfer, friction factor and thermal performance results. *Renew. Energy* **2000**, *19*, 379–398. [\[CrossRef\]](#)
- El Nady, J.; Kashyout, A.; Ebrahim, S.; Soliman, M. Nanoparticles Ni electroplating and black paint for solar collector applications. *Alex. Eng. J.* **2016**, *55*, 723–729. [\[CrossRef\]](#)
- Hellstrom, B.; Adsten, M.; Nostell, P.; Karlsson, B.; Wackelgard, E. The impact of optical and thermal properties on the performance of flat plate solar collectors. *Renew. Energy* **2003**, *28*, 331–344. [\[CrossRef\]](#)
- Gowtham, G.; Kishan, P.; Natarajan, M. Prediction of most appropriate models for estimating monthly average daily global radiation in Vellore. In Proceedings of the 2013 International Conference on Energy Efficient Technologies for Sustainability (ICEETS), Nagercoil, India, 10–12 April 2013; pp. 607–610. [\[CrossRef\]](#)
- Korachagaon, I.; Bapat, V.N. Global solar radiation estimation by Irranna-Bapat's models for India. In Proceedings of the 2012 International Conference on Computing, Electronics and Electrical Technologies (ICCEET), Nagercoil, India, 21–22 March 2012; pp. 394–398. [\[CrossRef\]](#)
- Gangane, S.D. Economical Solar Water Heater. *IOSR J. Mech. Civ. Eng.* **2017**, *17*, 68–71. [\[CrossRef\]](#)
- Ertekin, C.; Kulcu, R.; Evrendilek, F. Techno-economic analysis of solar water heating systems in Turkey. *Sensors* **2008**, *8*, 1252–1277. [\[CrossRef\]](#) [\[PubMed\]](#)
- Chen, C.; Diao, Y.; Zhao, Y.; Wang, Z.; Zhu, T.; Wang, T.; Liang, L. Numerical evaluation of the thermal performance of different types of double glazing flat-plate solar air collectors. *Energy* **2021**, *233*, 121087. [\[CrossRef\]](#)
- Bakari, R.; Minja, R.J.A.; Njau, K.N. Effect of Glass Thickness on Performance of Flat Plate Solar Collectors for Fruits Drying. *J. Energy* **2014**, *2014*, 247287. [\[CrossRef\]](#)
- Salazar, A.; Rios, I. *Sustainable Agriculture: Technology, Planning and Management*; Nova Science Pub Inc.: New York, NY, USA, 2010.

19. Gopinathan, K.K. A General Formula for Computing the Coefficients of the Correlation Connecting Global Solar Radiation to Sunshine Duration. *Sol. Energy* **1988**, *41*, 499–502. [[CrossRef](#)]
20. Kumar, A.; Ferdous, R.; Luque-Ayala, A.; McEwan, C.; Power, M.; Turner, B.; Bulkeley, H. Solar energy for all? Understanding the successes and shortfalls through a critical comparative assessment of Bangladesh, Brazil, India, Mozambique, Sri Lanka and South Africa. *Energy Res. Soc. Sci.* **2019**, *48*, 166–176. [[CrossRef](#)]
21. Makade, R.G.; Chakrabarti, S.; Jamil, B. Prediction of global solar radiation using a single empirical model for diversified locations across India. *Urban Clim.* **2019**, *29*, 100492. [[CrossRef](#)]
22. Samanta, S.; Patra, P.K.; Banerjee, S.; Narsimhaiah, L.; Chandran, M.A.S.; Kumar, P.V.; Bandyopadhyay, S. Generation of common coefficients to estimate global solar radiation over different locations of India. *Theor. Appl. Clim.* **2019**, *136*, 943–953. [[CrossRef](#)]
23. Sukhatme, S.P.; Nayak, J.K. *Solar Energy Principles of Thermal Collection and Storage*, 3rd ed.; Tata McGraw Hill Education Private Limited: New Delhi, India, 2008.
24. Mousavi Maleki, S.A.; Hizam, H.; Gomes, C. Estimation of hourly, daily and monthly global solar radiation on inclined surfaces: Models re-visited. *Energies* **2017**, *10*, 134. [[CrossRef](#)]
25. Disaster Management Draft Revised Goals 2017 | Vellore District, Government of Tamil Nadu | India. Available online: <https://vellore.nic.in/document/disaster-management-draft-revised-goals-2017/> (accessed on 16 September 2020).
26. Office of Management and Budget (OMB). *Standards and Guidelines for Statistical Surveys*; OMB: Washington, DC, USA, 2006.
27. IS 12933-5 (2003); Solar Flat Plate Collector, Part 5: Test Methods [MED 4: Non-Conventional Energy Sources]. Bureau of Indian Standards: Delhi, India, 2003.
28. Qureshy, A.M.M.I.; Dincer, I. Energy and exergy analyses of an integrated renewable energy system for hydrogen production. *Energy* **2020**, *204*, 117945. [[CrossRef](#)]
29. Ge, Z.; Wang, H.; Wang, H.; Zhang, S.; Guan, X. Exergy analysis of flat plate solar collectors. *Entropy* **2014**, *16*, 2549–2567. [[CrossRef](#)]
30. Popiel, C.O.; Wojtkowiak, J. Simple formulas for thermophysical properties of liquid water for heat transfer calculations (from 0 °C to 150 °C). *Heat Transf. Eng.* **1998**, *19*, 87–101. [[CrossRef](#)]
31. Eltaweel, M.; Abdel-Rehim, A.A.; Attia, A.A. A comparison between flat-plate and evacuated tube solar collectors in terms of energy and exergy analysis by using nanofluid. *Appl. Therm. Eng.* **2021**, *186*, 116516. [[CrossRef](#)]
32. Yang, M.H. Payback period investigation of the organic Rankine cycle with mixed working fluids to recover waste heat from the exhaust gas of a large marine diesel engine. *Energy Convers. Manag.* **2018**, *162*, 189–202. [[CrossRef](#)]
33. Dwivedi, V.K.; Tiwari, G.N. Thermal modeling and carbon credit earned of a double slope passive solar still. *Desalination Water Treat.* **2010**, *13*, 400–410. [[CrossRef](#)]
34. Prabhakant; Tiwari, G.N. Evaluation of carbon credits earned by energy security in India. *Int. J. Low-Carbon Technol.* **2009**, *4*, 42–51. [[CrossRef](#)]
35. Wong, J.H.; Royapoor, M.; Chan, C.W. Review of life cycle analyses and embodied energy requirements of single-crystalline and multi-crystalline silicon photovoltaic systems. *Renew. Sustain. Energy Rev.* **2016**, *58*, 608–618. [[CrossRef](#)]
36. Li, D.; Zhou, L.; Wang, X.; He, L.; Yang, X. Effect of crystallinity of polyethylene with different densities on breakdown strength and conductance property. *Materials* **2019**, *12*, 1746. [[CrossRef](#)]
37. Kiessling, A.; Simavilla, D.N.; Vogiatzis, G.G.; Venerus, D.C. Thermal conductivity of amorphous polymers and its dependence on molecular weight. *Polymer* **2021**, *228*, 123881. [[CrossRef](#)]
38. Tropin, T.V.; Schulz, G.; Schmelzer, J.W.P.; Schick, C. Heat capacity measurements and modeling of polystyrene glass transition in a wide range of cooling rates. *J. Non-Cryst. Solids* **2015**, *409*, 63–75. [[CrossRef](#)]
39. Borhani Zarandi, M.; Bioki, H.A.; Mirbagheri, Z.A.; Tabbakh, F.; Mirjalili, G. Effect of crystallinity and irradiation on thermal properties and specific heat capacity of LDPE & LDPE/EVA. *Appl. Radiat. Isot.* **2012**, *70*, 1–5. [[CrossRef](#)] [[PubMed](#)]
40. Dondapati, R.S.; Agarwal, R.; Saini, V.; Vyas, G.; Thakur, J. Effect of Glazing Materials on the Performance of Solar Flat Plate Collectors for Water Heating Applications. *Mater. Today Proc.* **2018**, *5*, 27680–27689. [[CrossRef](#)]
41. ISO 9050:2003; Glass in Building—Determination of Light Transmittance, Solar Direct Transmittance, Total Solar Energy Transmittance, Ultraviolet Transmittance and Related Glazing Factors. International Organization for Standardization: Geneva, Switzerland, 2003. Available online: <https://www.iso.org/standard/35062.html> (accessed on 31 August 2020).
42. Choi, Y.; Mae, M.; Kim, H.B. Thermal performance improvement method for air-based solar heating systems. *Sol. Energy* **2019**, *186*, 277–290. [[CrossRef](#)]
43. Xiaowu, W.; Ben, H. Exergy analysis of domestic-scale solar water heaters. *Renew. Sustain. Energy Rev.* **2005**, *9*, 638–645. [[CrossRef](#)]
44. Koussa, M.; Saheb, D.; Belkhamisa, H.; Lalaoui, M.A.; Hakem, S.A.; Sami, S.; Zoubir, B.; Mustapha, H. Effect of parallel and serie connection configuration of solar collector on the solar system performances. In Proceedings of the 2015 6th International Renewable Energy Congress (IREC 2015), Sousse, Tunisia, 24–26 March 2015; Institute of Electrical and Electronics Engineers Inc.: Piscataway Township, NJ, USA, 2015. [[CrossRef](#)]
45. Mohammed, A.K.; Hamakhan, I.A. Analysis of energy savings for residential electrical and solar water heating systems. *Case Stud. Therm. Eng.* **2021**, *27*, 101347. [[CrossRef](#)]
46. Guidelines on Implementation of Phase-II of Grid Connected Rooftop Solar Programme for Achieving 40 GW Capacity from Rooftop Solar by the Year 2022. Available online: www.solarrooftop.gov.in (accessed on 21 September 2020).

47. Wellford, B.W. *Calculating the Efficiency of Energy Recovery Ventilation and its Effect on Efficiency and Sizing of Building HVAC Systems*; AHRI: Arlington, VA, USA, 2011.
48. Rao, V.T.; Sekhar, Y.R. Comparative analysis on embodied energy and CO₂ emissions for stand-alone crystalline silicon photovoltaic thermal (PVT) systems for tropical climatic regions of India. *Sustain. Cities Soc.* **2022**, *78*, 103650. [[CrossRef](#)]
49. Chauhan, P.S.; Kumar, A.; Nuntadusit, C. Thermo-environmental and drying kinetics of bitter melon flakes drying under north wall insulated greenhouse dryer. *Sol. Energy* **2018**, *162*, 205–216. [[CrossRef](#)]
50. Shrivastava, V.; Kumar, A. Embodied energy analysis of the indirect solar drying unit. *Int. J. Ambient. Energy* **2017**, *38*, 280–285. [[CrossRef](#)]
51. Alsabri, A.; Al-Ghamdi, S.G. Carbon footprint and embodied energy of PVC, PE, and PP piping: Perspective on environmental performance. *Energy Rep.* **2020**, *6*, 364–370. [[CrossRef](#)]
52. Sharma, M.; Atheaya, D.; Kumar, A. Performance evaluation of indirect type domestic hybrid solar dryer for tomato drying: Thermal, embodied, economical and quality analysis. *Therm. Sci. Eng. Prog.* **2023**, *42*, 101882. [[CrossRef](#)]

Disclaimer/Publisher’s Note: The statements, opinions and data contained in all publications are solely those of the individual author(s) and contributor(s) and not of MDPI and/or the editor(s). MDPI and/or the editor(s) disclaim responsibility for any injury to people or property resulting from any ideas, methods, instructions or products referred to in the content.